



Porous biomorphic ceramics for catalytic decomposition of phenol

Gaida Sedmale^a, Maris Rundans^{a,*}, Martins Randers^a, Liga Grase^a, Aija Krumina^b

^a Institute of Silicate Materials, Riga Technical University, Paula Valdena str. 3, LV-1048, Riga, Latvia

^b Institute of Inorganic Chemistry, Riga Technical University, Paula Valdena str. 7, LV-1048, Riga, Latvia



ARTICLE INFO

Keywords:
Ceramics
Illite clay
Templates

ABSTRACT

Porous ceramics have been developed from lichen templates infiltrated with illite clay slurry and mineralized at 900 °C in air and nitrogen environments. The obtained ceramic samples were thoroughly investigated as well as tested for phenol catalytic decomposition ability. The structures of mineralized samples in air and nitrogen environments differ; samples mineralized in air demonstrate poorly structured platelets of plagioclase and mainly quartz, as well as small amorphous areas. The presence of crystalline particles in sizes from 400 up to 850 nm and attributed to carbon or iron is typical for samples mineralized in nitrogen. The effect on phenol catalytic decomposition can be evaluated as 80% effective decomposition after contact of samples with phenol-water solution. One of the main factors for catalytic decomposition of phenol is considered to be the presence of differently located Fe³⁺,²⁺ ions in the structure of samples with the decomposition process being akin to Fenton reactions.

1. Introduction

Biomorphic mineralization is a relatively widely studied process by which new materials are obtained using natural templates in combination with synthetic compounds. The products, biomorphic materials, combine natural geometry with synthetic material chemistry, e.g., Ref. [1–4]. Through synthesis or assembly using a wide range of natural templates from nano-to micro-to mega-scale dimensions, including biomolecules, microorganisms, plants, animals origin materials, a wide range of materials for different uses can be developed [5–13].

There are two separate types of biomorphic mineralization processes: one consumes the template and converts it into biomorphic material; that is, the template itself is a reagent and contributes to the final product; second, biomorphic materials are formed as a result of mineralization of precursors deposited on the template.

Wood is one of the most commonly used cellular and anisotropic materials for the second type of biomorphic process. Wood templates are derived, notably, from cellulose-rich plants, mainly trees. Wood exhibits microstructural features ranging from millimetre down to nanometre scale (molecular cell patterns, macro- and micro-cell structures) [14,15]. Attempts have been made to produce ceramics derived from wood tissues and these ceramics generally inherit the morphology and microstructure of the wood and present properties like light weight, good mechanical strength, and a large surface area. It is shown that the process of

fabrication of wood template ceramics includes three steps: the formation of a bio-carbon template by pyrolyzation of wood materials, infiltration of the template with ceramic precursors, and calcination to form ceramics and remove organic materials. Carbides are the most reported ceramic materials and can be synthesized by various routes, but mainly by liquid infiltration using Si-containing organic sols followed by a high-temperature reaction, e.g., Refs. [16,17].

In [18] showed that biomorphic composite ceramics can also be produced with second phase precursor by infiltrating the cellular SiC wood ceramic with ZrO₂ sols. On the other hand [19,20], zeolite wood ceramics composite can be developed via zeolitization of wood tissues or wood ceramics, especially wood ceramics with high silicon content.

Despite the fact that plants are a diverse group of living things with widely different morphologies that can be used for biomorphic mineralization, a big group of inorganic templates can also be named, for example sedimentary deposits of diatomites. The diatomite group provides diverse complicated structures with nano-scaled features for healthcare, e.g. Ref. [21].

As shown, biomorphic mineralization offers ample opportunities for the development of new materials. The most widely applied template materials and products obtained have been collected by Ref. [1] and are summarized in Table 1.

The process of biomorphic mineralization includes various methods which can be roughly classified into two types: chemical and physical

* Corresponding author.

E-mail addresses: gaida-maruta.sedmale@rtu.lv (G. Sedmale), maris.rundans@rtu.lv (M. Rundans), martins.randers@rtu.lv (M. Randers), liga.grase@rtu.lv (L. Grase), aija.krumina@rtu.lv (A. Krumina).

<https://doi.org/10.1016/j.oceram.2020.100024>

Received 13 July 2020; Received in revised form 16 September 2020; Accepted 28 September 2020

Available online 19 October 2020

2666-5395/© 2020 The Author(s). Published by Elsevier Ltd on behalf of European Ceramic Society. This is an open access article under the CC BY-NC-ND license

(<http://creativecommons.org/licenses/by-nc-nd/4.0/>).

Table 1
Biomorphic materials templated by plant materials.

Plant materials	Biomorphic materials
Wood tissue	Porous carbides, porous metal oxides, nitrides, composites: SiC/C, Al ₂ O ₃ , TiC/C, SiSiC/zeolite, SiSiC/Al-Si, etc.
Bamboo	Porous SiC ceramics
Maize	Porous SiC ceramics
Pollen grains	Porous SiO ₂ , CaCO ₃ , calcium phosphate ceramics
Diatomite	Nano-structured metal oxides, metals, silica, carbon, carbide, nitride, etc.

routes. Therefore, if it is necessary to achieve a good reproduction of natural structures, a liquid precursor is favourable, because it may provide a good wetting between template and precursor. Considering advantages like chemical flexibility, shape control, and mild reaction conditions, the sol-gel method is most suitable. The sol-gel process can be applied to most of the templates: viruses, diatomites, cellulose, silk, wood tissues, eggshells, butterfly wings, and so on. Metal-containing solutions (metal salts, metal alkoxides) are similar, e.g., Ref. [22,23].

Wet method precipitation is more often applied, mainly for metals and alloys, by using a wide range of templates, such as biomolecules, silk, eggshells, plants, and so forth [24,25]. Other known methods used include reactive melt infiltration, chemical vapour deposition or infiltration, etc. Similar to the wet method, wet precipitation of clay, silica, and calcite nanoparticles on wood [26], cellulose [27,28], moss, lichen, and so on can also be considered. There are few studies that focus on the use of clay or silica nanoparticles for the production of biomorphic mineralized materials. In this case, biomorphic materials are formed as a result of mineralization of precursors deposited on the template.

Table 2
Chemical composition and granulometric data of the used clay.

	SiO ₂	Al ₂ O ₃	Fe ₂ O ₃	TiO ₂	CaO	MgO	K ₂ O	Na ₂ O	Ignition loss (at 1000 °C)
Clay (wt.%)	46.87	18.74	7.06	0.59	6.62	3.25	3.62	0.41	12.84
Chemically separated illite (wt.sh.)	44.0	19.7	10.3	0.8	0.6	2.3	5.3	0	–
Sand fraction	Aleirite (dust) fraction		Clay mineral fraction*						
>50 μm	50–5 μm		<5 μm int. al.						
1.33	8.67		90.00						
			< 2 μm						
			60.60						

This work is focused on development of biomorphic porous ceramics by use of lichen as natural template infiltrated with illite clay nanoparticles and mineralized at elevated temperatures to assess its suitability for the catalytic decomposition of phenol in contaminated waters.

2. Materials and methods

The main starting materials were illite clay samples taken from the clay deposit of Quaternary period, Baltic stratum (Latvia) from a soil depth of 2–3 m. For the investigations, an intermediate composition of illite clay and illite mineral fraction was used. The separation of illite mineral fraction was performed using the chemical method in accordance with Kostjukovs et al. [29]. The chemical and granulometric composition of illite clay as well chemical composition of separated illite mineral fraction is shown in Sedmale et al. [30] and Table 2.

The phase transition by heating of raw clay material was analysed with differential thermal analysis (DTA) equipment (Setaram, Setsys Evolution 1750) at temperatures ranging from room temperature to 1000 °C and a heating rate of 10 °C/min. These transitions are shown on differential thermal analysis-thermogravimetric curves, Fig. 1.

The technological approaches used for the formation and investigation of mineralized cellular ceramic samples included the following steps and objectives, which are typical for conventional ceramic technology:

- preparation of 40–45% water–clay nanoparticles slurry from illite or illite clay during 1–3 h by milling/homogenization in a planetary mill (PM100). It was found that the specific surface area of particles changed very little depending on the time of milling (the average size of particles in slurry was calculated to be approximately 100 nm),

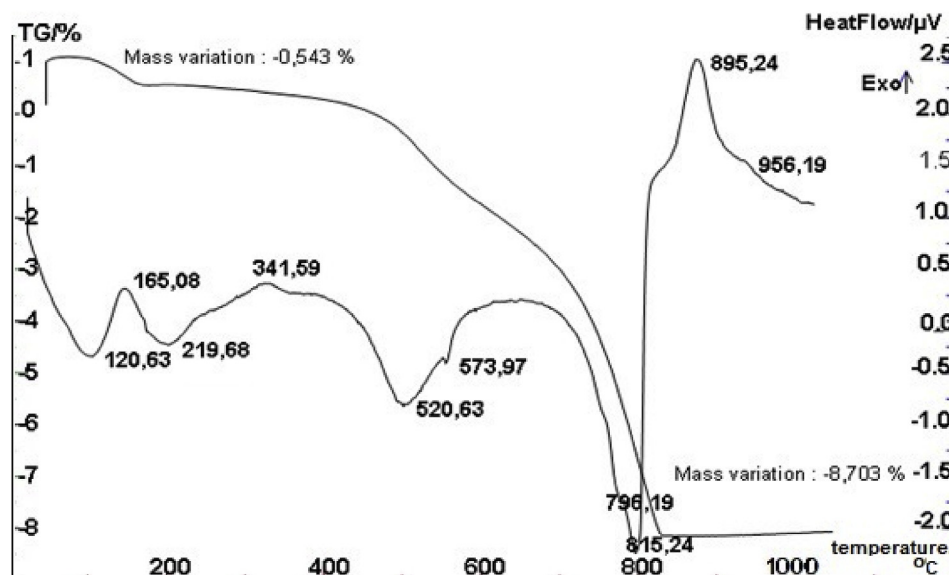


Fig. 1. Differential thermal analysis-thermogravimetric (DTA-TG) curves of used raw clay.

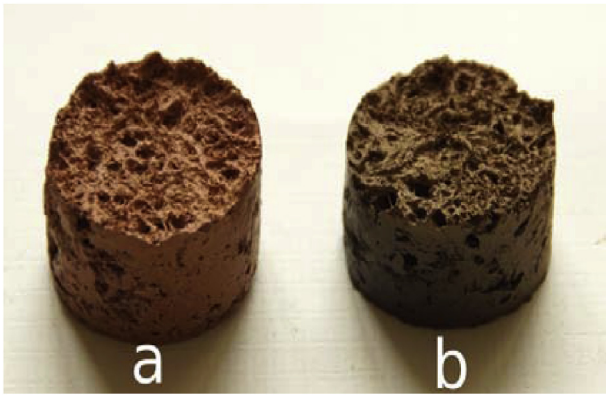


Fig. 2. Photographs of biomorphic ceramics samples sintered at 900 °C by use of lichen as template after mineralization in: a) air environment and b) in nitrogen.

- preparation of lichen (*Evernia Prunastri*) templates by washing in water and drying afterwards,
- shaping of cylindrical ($h = 25\text{--}28\text{ mm}$, $\varnothing = 20\text{ mm}$) or rectangular ($20 \times 30 \times 10\text{ mm}$) raw samples by infiltration of slurry into templates during 24 h of treatment followed by drying (the mass ratio of dry lichen – illite clay in slurry changed to limits 1:1 to 1:4),
- mineralization-sintering of dried samples at temperatures at 800, 900, and 1000 °C in air and in a nitrogen environment using a Nabertherm furnace,
- investigation of the bulk density (measured by the Archimedes method with an accuracy of $\pm 0.5\%$ using distilled water medium and paraffinized samples) and compressive strength (determined by ToniNorm 2020 from Toni Technik) of mineralized samples. The values of these properties were calculated from three parallel measurements of each sample, but it should be noted that due to the varying sample sizes, which deviate from the standard, the acquired values of compressive strength are approximate.

Table 3

Specific surface areas of pore fraction of mineralized samples.

Samples mineralized at 900 °C in	Pore fraction	Surface area, m^2/g
air environment	1.15–2.95 nm	3.80
	1.05–9.90 μm	6.15
nitrogen environment	1.10–8.50 nm	7.25
	6.60–9.95 μm	10.80

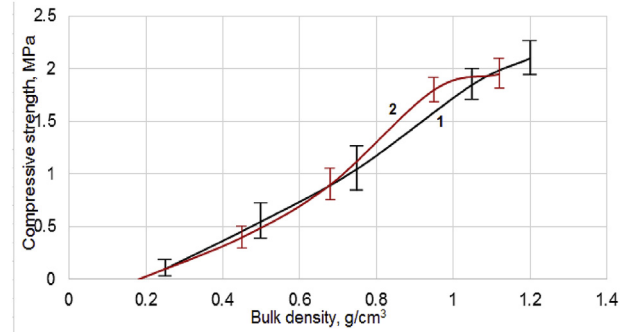


Fig. 4. Compressive strength vs. bulk density of samples mineralized at 900 °C: 1 – in air environment, 2 – in nitrogen.

The phase compositions of sintered-mineralized samples were determined by X-ray diffraction (XRD) apparatus (D8 Advance, Bruker, with $\text{CuK}\alpha$ radiation in a scanning interval of $2\theta = 10\text{--}60^\circ$ and scanning speed of $4^\circ/\text{min}$) and the structure was determined by scanning electron microscopy (SEM, Nova NanoSEM 650, The Netherlands). An image-processing program (ImageJ) was used to determine the average size of particles [31]. The size of particles was calculated as the average of 30 measurements.

Fourier transform infrared spectroscopy (FTIR, Prestige Shimadzu Corp., 21FTIR-8400S) was applied to detect typical link fluctuations in samples.

The pore distribution analysis was performed by the nitrogen adsorption (BET) and mercury intrusion methods by use of

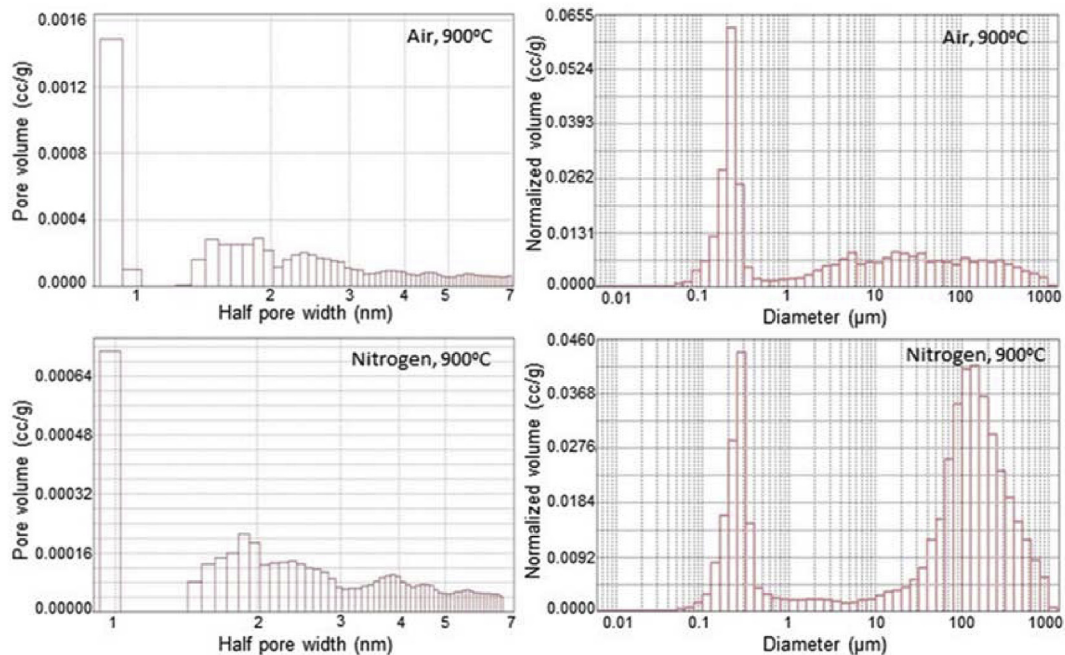


Fig. 3. The histograms of pore distribution of biomorphic ceramic samples, sintered in an air environment and in nitrogen at temperature 900 °C, performed by the nitrogen adsorption (left) and mercury intrusion methods (right).

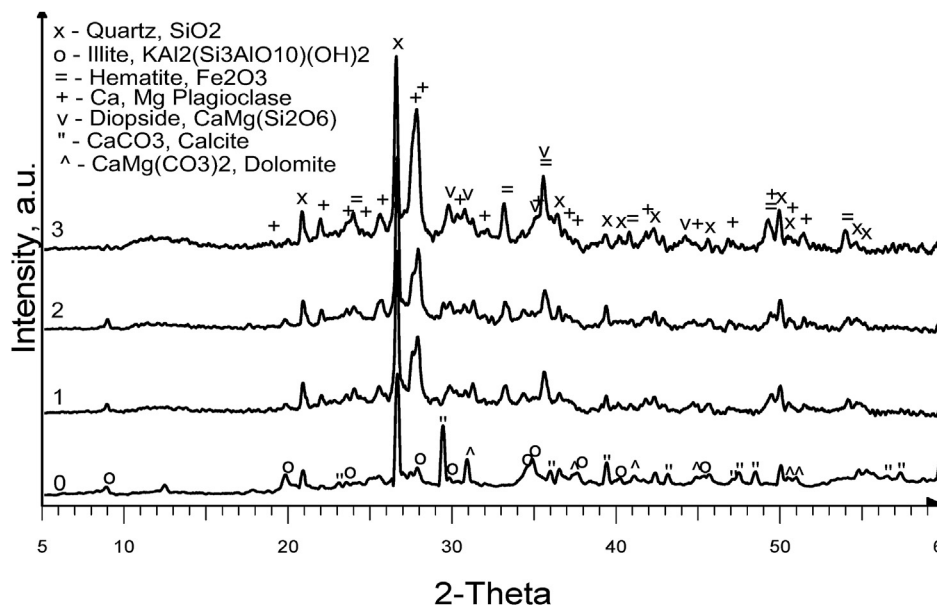


Fig. 5. XRD patterns of samples mineralized at 800 °C (1), 900 °C (2), and 1000 °C (3) in an air environment, as well as raw illite clay samples (0).

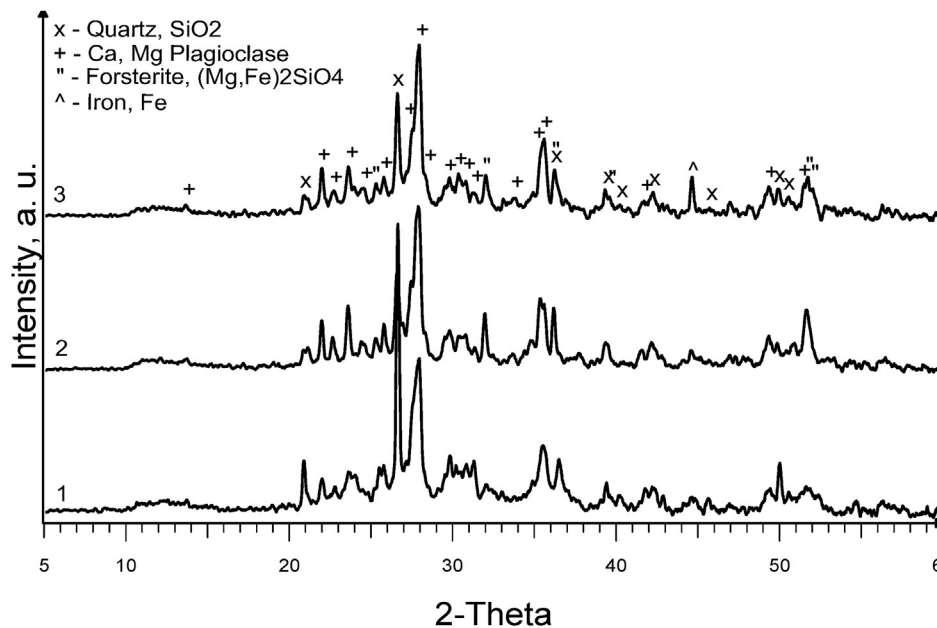


Fig. 6. XRD patterns of samples mineralized at 800 °C (1), 900 °C (2), and 1000 °C (3) in a nitrogen environment.

Quantachrome Nova 1200e Surface Area and Pore Size Analyzer. Specific surface areas of mineralized samples were calculated of the data obtained by the nitrogen adsorption (BET) and mercury intrusion methods.

Experimental set up for catalytic decomposition of phenol by use of the biomorphic ceramics samples as phenol-decomposing material was as follows: a 500 ml capacity glass vessel with an adjustable temperature controller and magnetic stirrer was used for the experiments. The 470 ppm phenol-water solution (50 ml) and 4 ml 0.5% H_2O_2 solution was added to the vessel used for each test. Ceramic samples were immersed into phenol-water solution and stirred for different durations at 70–75 °C. After the end of the experiment, a sample of the solution was placed into a quartz cell and the change in the phenol content was determined from the characteristic absorption peak at 270 nm by use of a spectrophotometer (Genesis 10S UV and Visionlite program). In addition measurement of the chemical oxygen demand (COD) for the

decomposition of phenol in accordance with [32], as well as pH value determination by use of pH-meter (Hanna Instrument) was also performed.

3. Results and discussion

The processes that occur during the heating of illite mineral fraction and illite clay in the temperature range from room temperature to 1000 °C are similar for both [30]. The main processes of heating could be characterized by endothermic effects occurring at temperatures between 120 and 219 °C and at 520 °C and are related (accordingly) to weakly associated water and the withdrawal of structural water. This process is accompanied by a relatively large weight loss. Weakly pronounced effect at 573 °C is associated with changing $\alpha \rightarrow \beta$ modifications of quartz. At temperatures >600 °C a liquid phase starts to form, and simultaneously,

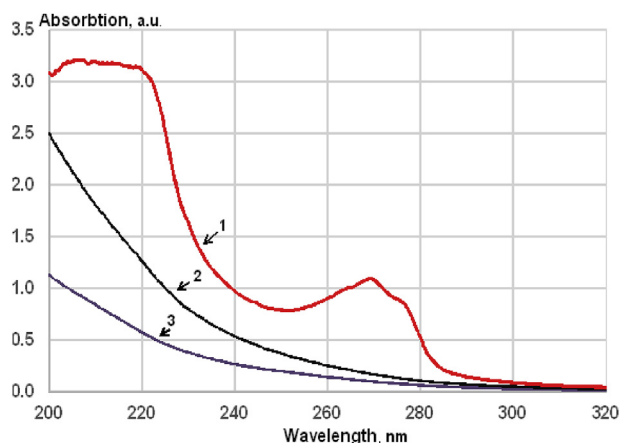


Fig. 7. Comparative results of UV spectra after contact of biomorphic cellular ceramics samples mineralized in an air (curve 3) and in a nitrogen environment (curve 2) with starting phenol-water solution (curve 1).

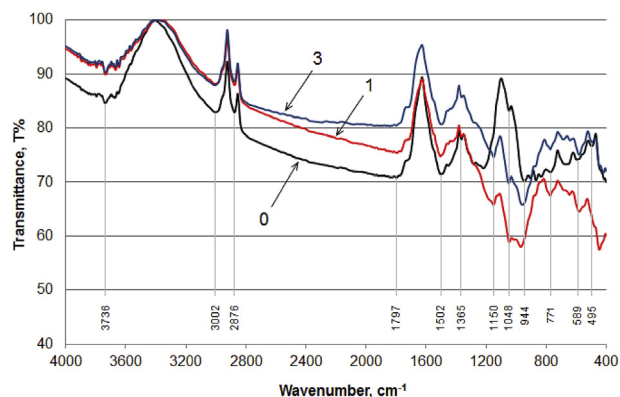


Fig. 8. FTIR spectra of raw (0) and samples mineralized at 900 °C in air (1) and in nitrogen (3).

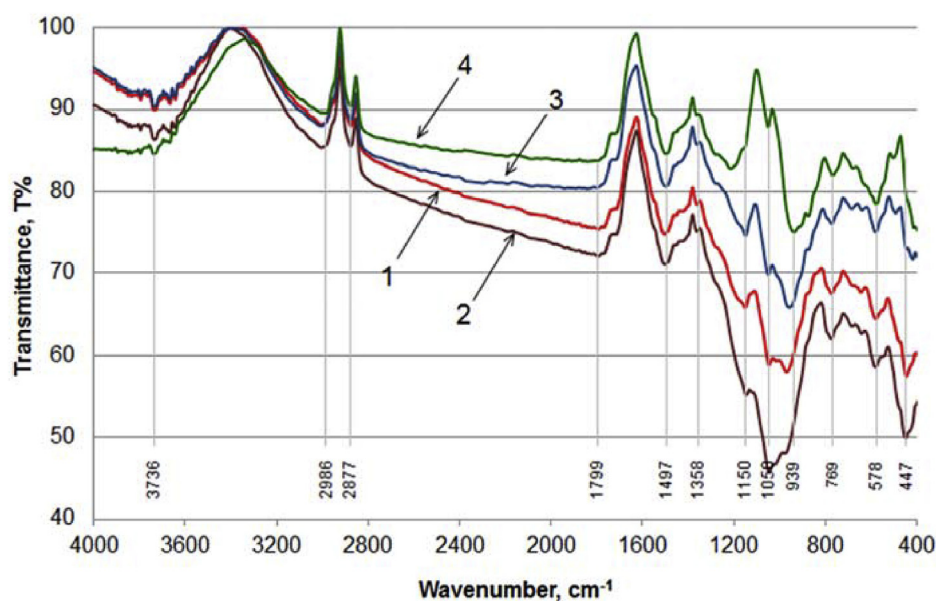


Fig. 9. Comparative FTIR spectrum of mineralized samples at temperature 900 °C in air (curves 1 and 2) and in nitrogen (curves 3 and 4); before contact – curves 1 and 3; after contact with phenol-water solution for 140 min. – curves 2 and 4.

a weakly pronounced exothermic process of formation of new phases occurs.

By the mineralizing of infiltrated templates there are formed samples - biomorphic ceramic which reflects natural geometry of used lichen. Template in this process decompose promoting the formation of the gaseous phase creating pore development As an optimal temperature was chosen here 900 °C (lower than melting temperature of the clay) both for mineralizing in air and nitrogen environment, which could provide acceptable mechanical strength, pore volume and distribution of samples, whereas the choice of the nitrogen environment during mineralizing process was associated with the formation of reduced forms of components of sample who could contribute to the catalytic process.

Fig. 2 shows the photographs of the mineralized at temperature 900 °C in air environment and nitrogen biomorphic ceramics samples.

Visually, ≥ 2 mm cells/voids in the presence of wide range of pores can be observed, as is shown in **Fig. 2**. The theoretical calculated porosity is up to 70% for in an air and up to 65% for in a nitrogen mineralized samples.

As shown (**Fig. 3**) pore distribution both in the nanoscale range, and range of 0.10 μm –10 μm for in an air and nitrogen mineralized samples in approximation are similar. Considerable difference appears for sample mineralized in nitrogen in the largest pore range (10 μm –1000 μm) which is linked to a significant gaseous phase formation, both breaking down the template material (this process apparently dominates by the mineralization of samples in the air environment) and the structure of the clay minerals, which in turn is determined mainly by changing Fe ion valence (as an additional process of formation of the gaseous phase to above mentioned). The results of specific surface areas of pore fraction of mineralized samples in air and in nitrogen are shown in **Table 3**.

The samples have relatively low bulk density and compressive strength; the average values of these characteristics for sample mineralized at 900 °C by changing weight ratio between the clay and the template (i.e., bulk density) is shown in **Fig. 4**. The value of compressive strength up to 2 MPa was reached at mass ratio of lichen–clay 1:3 if mineralization was performed in air. Additional porosity is developed by mineralization in nitrogen environment under the same conditions which causes the compressive strength to decrease.

The XRD of samples mineralized in an air environment (**Fig. 5**) shows the main diffraction reflexes characteristic for illite clay ceramic, namely

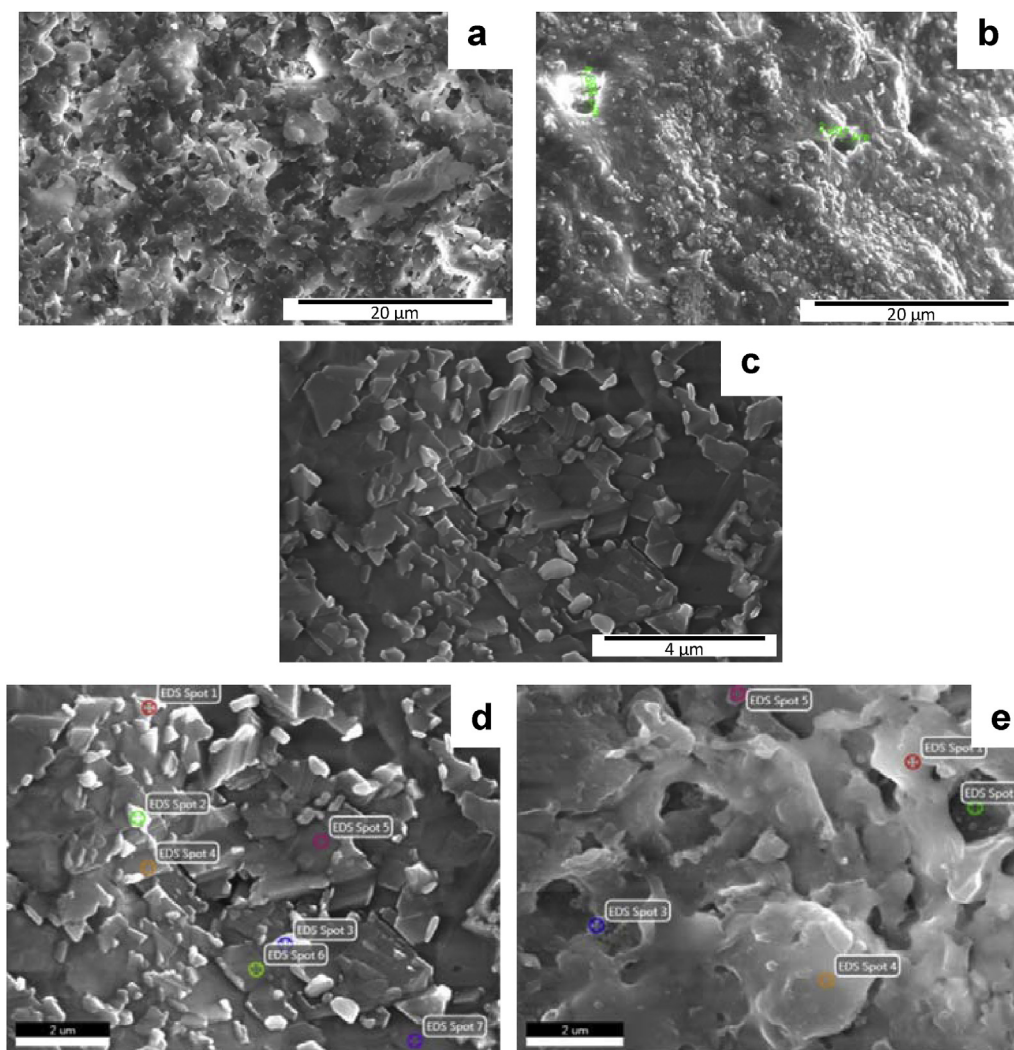


Fig. 10. SEM micrographs of lichen samples mineralized at 900 °C in air (a) and nitrogen (b, c). Spots revealed by EDS analysis of samples mineralized in nitrogen (d) and in air (e).

Table 4
The results of EDS analysis.

Lichen sample mineralized at 900 °C in nitrogen (Fig. 8d, Spot 2)			Lichen sample mineralized at 900 °C in air (Fig. 8e, Spot 3)		
Element	Weight %	Atomic %	Element	Weight %	Atomic %
C	2.05	3.57	C	1.56	2.85
O	44.08	63.05	O	41.49	56.81
Na	1.52	1.52	Na	0.76	0.72
Mg	2.93	2.76	Mg	3.65	3.29
Al	10.52	8.93	Al	11.85	9.62
Si	14.87	12.12	Si	23.33	18.2
P	–	–	P	0.36	0.26
K	1.2	0.7	K	2.33	1.86
Ca	6.92	3.95	Ca	6.66	3.64
Fe	16.32	6.69	Fe	7.01	2.75

quartz, haematite, and the newly formed phases $\text{CaMg}(\text{Si}_2\text{O}_6)$ diopside and Ca–Mg plagioclase.

However, the XRD patterns (Fig. 6) of samples mineralized in a nitrogen environment are different. New diffraction reflexes of iron and solid solution enriched with Fe ion containing forsterite appears.

It should be noted that during mineralization in a nitrogen environment, the illite phase is remarkably diminishing already at 800 °C, yet it persists as weak peaks (at 2-theta up to 8°, 20° degree) even in 900 °C air

environment obtained samples, as it is shown on Fig. 3 (reflexes at 2-theta = 8°, 20°, 34°). On both XRD patterns (Figs. 5 and 6), the presence of amorphous phase can also be observed as a small curvature by up to $2\theta = 25\text{--}30^\circ$, linked to the presence of carbon nanoparticles (as indicated by EDS analysis) as traces from template. From a catalytic (sorption) point of view remainders of the illites nanoparticles in mineralized samples could be viewed as positive contribution; it can be concluded from photometry results of changes of UV spectra after contact of samples mineralized in air (curve 1) and nitrogen (curve 2) environment with phenol-water solution (Fig. 7).

The FTIR spectra of both samples mineralized at a temperature of 900 °C in air and in nitrogen environments (Fig. 8) along with the raw clay samples show the typical spectrum of raw and thermally treated illite clay. Insignificant changes in the illite structure, characterized as changes in stretching bands at frequencies of up to 3750 cm^{-1} which can be attributed to the stretching of hydroxyl groups found at the edges of illite platelets are shown [33–36].

The small changes (comparing with raw clay) for the peaks to be marked at frequencies $3002\text{--}2800\text{ cm}^{-1}$ is attributed to the hydrogen bonds of the OH group [33,34].

The weak expanded signals in the range of frequencies of $1790\text{--}1612\text{ cm}^{-1}$ are applicable to physically adsorbed water molecules on illite platelets; this range is a little narrower for mineralized samples [37,38].

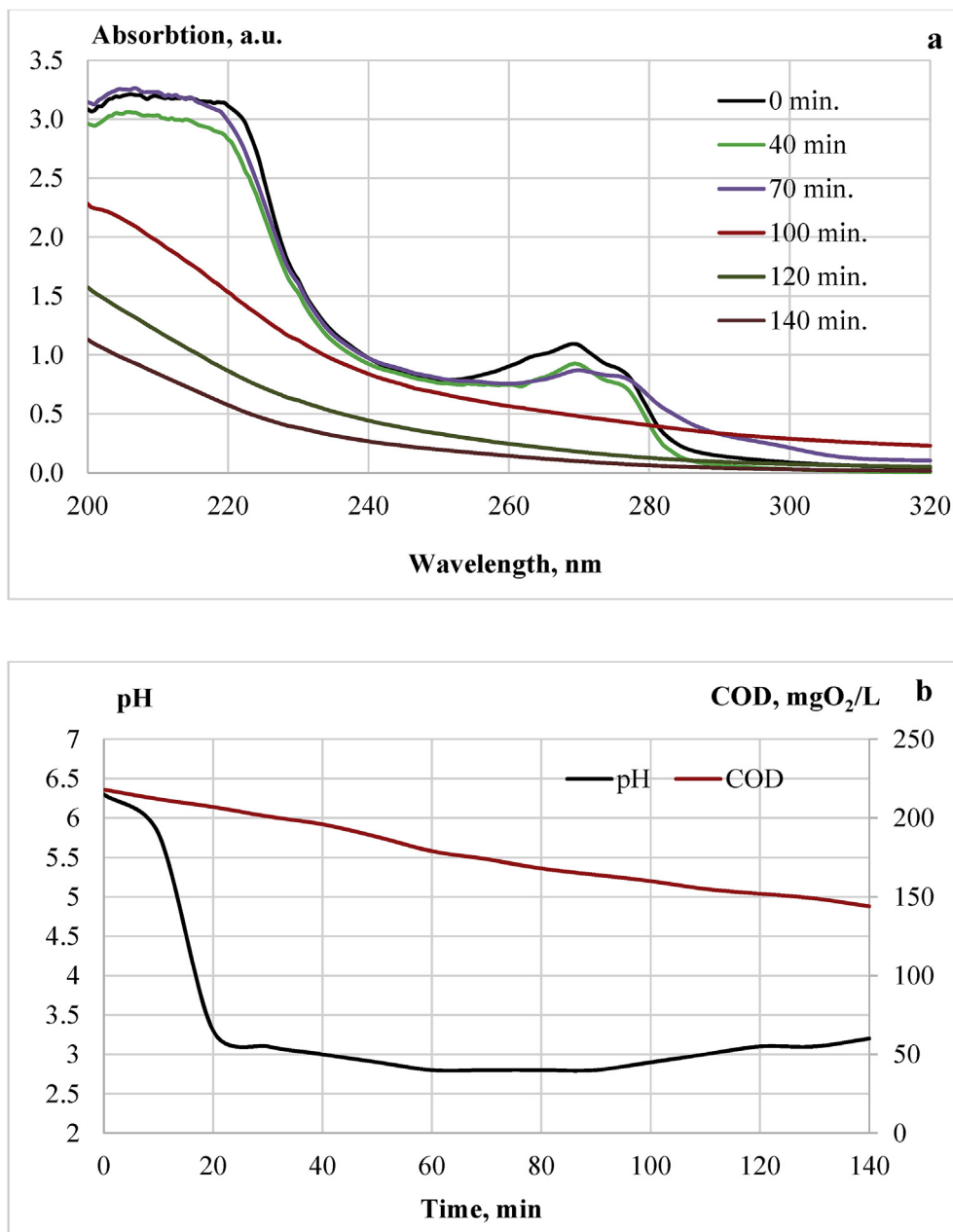


Fig. 11. The changes of UV-spectra (a), COD and pH (b) after contact of biomorphic ceramics sample sintered in air with phenol-water solution over time.

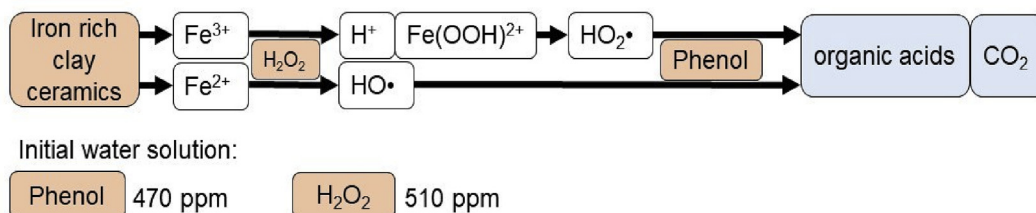


Fig. 12. Schematic description of the process of decomposition of phenol by applying its catalytic decomposition biomorphic ceramics sample.

The small bands at 1365 cm^{-1} are probably due to vibration modes of CO_3^{2-} groups and are most probably ascribable to residues of carbonates.

The absorption bands at 1150 , 1048 , and 944 cm^{-1} are related to the vibration of typical aluminosilicate's structural functions, including strong

bonds of Si-O at 1048 cm^{-1} and 944 cm^{-1} , while vibrations at 771 cm^{-1} more pronounced after mineralization is assigned to the Al-O-Si vibrations [36–39]. These results indicate that the 2:1 structure of the illites is slightly altered during the mineralization process, while maintaining the characteristics structural features.

It should be noted that vibrations related to the products of decomposition of lichen in the frequency range applied are not found.

Fig. 9 demonstrates the FTIR spectrum of samples after contact with phenol-water solution.

The small configuration change of the spectral lines in the minor frequency range 1150 cm^{-1} to 578 cm^{-1} can be observed here. This may be particularly attributed to Si–O vibrations of lines at 1150 cm^{-1} , 1050 cm^{-1} , 939 cm^{-1} , as well by 769 cm^{-1} and 578 cm^{-1} corresponding to Al–O–Si vibrations. From these results it could be concluded that samples are stable in the phenol-water solution while maintaining the outer shape as well as structure.

SEM microphotographs of the mineralized samples are shown on Fig. 10a, b, and c. As expected, the samples demonstrate poorly structured platelets of plagioclase and certain crystalline arrangements which could be attributed to quartz morphology; as a consequence of treatment, small amorphous areas and pores are observable on the surface of these platelets and between them.

More pronounced effects occur upon treatment in nitrogen, as can be seen in the sample on Fig. 10b and at higher magnification in Fig. 10c. Small crystalline formations that have been evenly placed on the surface of the platelets may be observed. They are clearly visible at higher magnification (Fig. 10c) but only for the sample mineralized in the nitrogen environment. The sizes of these crystalline formations differ. For less dense crystalline formations (grey), the size could be calculated as up to 400 nm on average; for bigger platelets it was $\sim 850\text{ nm}$ and even up to $2\text{ }\mu\text{m}$.

The estimated quantity of elements according to the results of EDS analysis of revealed spots is given in Table 4. Of particular interest is the growth of iron (Fe) as a reduced form of iron components of clay mainly in samples mineralized in nitrogen. This correlates with the growing intensity of the diffraction reflexes of Fe in the XRD pattern (Fig. 6, diffraction reflex at $2\text{-theta } 45^\circ$), which increases with mineralization temperature.

From the point of view of application, it may be accepted that the presence of iron (Fe) and carbon (C) particles in samples could be assessed positively.

The results of tests for reducing or eliminating the phenol decomposition in phenol-water solution as a function from time is shown (Fig. 11a) as changes of UV spectra over time as well as COD and pH of phenol-water solution (Fig. 11b) after contact with biomorphic porous ceramics sample sintered in air.

The process occurring there can be described schematically (Fig. 12) in the following and identical ways specified in the [40] where the degradation of tetracycline over Fe_3O_4 catalyst was studied by using Fenton reactions. This means, that in the process described here, the key role of the $\text{Fe}^{3+,2+}$ ions differently located in the biomorphic ceramic samples structure is one of the main factors for catalytic decomposition of phenol.

Despite the fact that these results mainly give qualitative input on effect of biomorphic cellular ceramics assessment, there is an obvious positive effect. It should be noted that in such processes taking place in the aquatic environment, reactions may continue to form new low-toxicity compounds. These compounds unfortunately in this stage interfere with ability to obtain reasonable quantitative results.

4. Summary and conclusions

High porosity biomorphic (cellular) ceramics can be produced using the natural templates (lichen) infiltrated by illite clay nanoparticles slurry and mineralized at different temperatures ranging from $800\text{ }^\circ\text{C}$ to $1000\text{ }^\circ\text{C}$ in air and nitrogen environments.

Mineralized at $900\text{ }^\circ\text{C}$ samples have high porosity (up to 65–70%) with pore size in range from $1\text{--}2\text{ nm}$ to $10\text{ }\mu\text{m}$ and visually visible $\geq 2\text{ mm}$ cells – voids. Their bulk density is up to 1.2 g/cm^3 and relatively low mechanical strength of $\sim 2\text{ MPa}$.

The crystalline phase compositions of samples are typical for illite

clay ceramics, but differs for both mineralized in an air and in a nitrogen environment. For air mineralized samples are characteristic the preservation of the illite phase to $900\text{ }^\circ\text{C}$, as well along with others phases – haematite Fe_2O_3 , which is almost unobserved for nitrogen-mineralized samples. Conversely there illite phase is very weak pronounced, but Fe phase formation is observed as the reduced form of Fe-oxides of clay.

The SEM structures of samples mineralized in the nitrogen environment show that the presence of different particles with sizes ranging from $2\text{ }\mu\text{m}$ to 850 nm and small crystalline formations of up to 400 nm there is typical. These crystalline formations correspond to carbon spots and iron.

Samples mineralized in an air consist of poorly structured platelets of plagioclase and certain crystalline arrangements which could be attributed to quartz structures; between them, small amorphous areas and pores are visible on the surfaces of platelets.

It is shown that the catalytic decomposition of phenol by use of mineralized samples sintered in air is in accordance with Fenton – reactions where the key role have the presence of the $\text{Fe}^{3+,2+}$ ions differently located in the structure of samples. During experiments the biomorphic ceramics samples maintain their shape and do not change their original weight and can be re-used and served for an extended period of time.

Declaration of competing interest

The authors declare that they have no known competing financial interests or personal relationships that could have appeared to influence the work reported in this paper.

Acknowledgements

This study has been carried out with financial support from the European Regional Development Fund under the project 1.1.1.1/16/A/077 “Mineral and Synthetic Nanopowders for Obtaining of Porous Ceramics and Modification of Ceramic Materials”.

References

- [1] T.X. Fan, S.K. Chow, D. Zhang, Biomimetic mineralization: from biology to materials, *Prog. Mater. Sci.* 54 (2009) 542–659, <https://doi.org/10.1016/j.pmatsci.2009.02.001>.
- [2] H. Sieber, Biomimetic synthesis of ceramics and ceramic composites, *Mater. Sci. Eng.* 412 (2005) 43–47, <https://doi.org/10.1016/j.msea.2005.08.062>.
- [3] T. Zhang, Y. Zhou, X. Bu, Y. Wang, M. Zhang, J. Hu, Fabrication of biomorphic Al₂O₃ ceramics with hierarchical architectures by templating of cotton fibers, *Ceram. Int.* 40 (2014) 13703–13707, <https://doi.org/10.1016/j.ceramint.2014.05.005>.
- [4] A.W. Xu, Y. Ma, H. Cölfen, Biomimetic mineralization, *J. Mater. Chem.* 17 (2007) 415–449, <https://doi.org/10.1039/b611918m>.
- [5] Q. Gu, C. Cheng, S. Suryanarayanan, K. Dai, D.T. Haynie, DNA-templated fabrication of nickel nanocluster chains, *Phys. E Low-dimens. Syst. Nanostruct.* 33 (2006) 92–98, <https://doi.org/10.1016/j.physe.2005.11.010>.
- [6] X. Gao, H. Matsui, Peptide-based nanotubes and their applications in bionanotechnology, *Adv. Mater.* 17 (2005) 2037–2050, <https://doi.org/10.1002/adma.200401849>.
- [7] V. Stsiapura, A. Sukhanova, A. Baranov, M. Artemyev, O. Kulakovich, V. Oleinikov, M. Pluot, J.H.M. Cohen, I. Nabiev, DNA-assisted formation of quasi-nanowires from fluorescent CdSe/ZnS nanocrystals, *Nanotechnology* 17 (2006) 581–587, <https://doi.org/10.1088/0957-4484/17/2/040>.
- [8] H. Zhou, T. Fan, D. Zhang, Hydrothermal synthesis of ZnO hollow spheres using spherobacterium as biotemplates, *Microporous Mesoporous Mater.* 100 (2007) 322–327, <https://doi.org/10.1016/j.micromeso.2006.11.020>.
- [9] B.E.L. Mayes, F. Vollrath, S. Mann, Fabrication of magnetic spider silk and other silk-fiber composites using inorganic nanoparticles, *Adv. Mater.* (1998) 801–805.
- [10] L. Huang, H. Wang, C.Y. Hayashi, B. Tian, D. Zhao, Y. Yan, Single-strand spider silk templating for the formation of hierarchically ordered hollow mesoporous silica fibers, *J. Mater. Chem.* 13 (2003) 666–668, <https://doi.org/10.1039/b212126c>.
- [11] T.J. Beveridge, M.N. Hughes, H. Lee, K.T. Leung, R.K. Poole, I. Savvaiddis, S. Silver, J.T. Trevors, Metal-microbe interactions: contemporary approaches, [https://doi.org/10.1016/s0065-2911\(08\)60158-7](https://doi.org/10.1016/s0065-2911(08)60158-7), 1997.
- [12] S.A. Davis, S.L. Burkett, N.H. Mendelson, S. Mann, Bacterial templating of ordered macrostructures in silica and silica-surfactant mesophases, *Nature* 385 (1997) 420–423, <https://doi.org/10.1038/385420a0>.
- [13] D. Zhang, L. Qi, Synthesis of mesoporous titania networks consisting of anatase nanowires by templating of bacterial cellulose membranes, *Chem. Commun.* (2005) 2735–2737, <https://doi.org/10.1039/b501933h>.

- [14] P. Greil, T. Lifka, A. Kaindl, Biomorph cellular silicon carbide ceramic from wood: II Mechanical Properties, *J. Eur. Ceram. Soc.* 18 (1998) 1961–1975.
- [15] M. Singh, B.M. Yee, Reactive processing of environmentally conscious, biomorphic ceramics from natural wood precursors, *J. Eur. Ceram. Soc.* 24 (2004) 209–217, [https://doi.org/10.1016/S0955-2219\(03\)00244-9](https://doi.org/10.1016/S0955-2219(03)00244-9).
- [16] T. Ota, M. Takahashi, T. Hibi, M. Ozawa, S. Suzuki, Y. Hikichi, Biomimetic process for producing SiC “wood”, *J. Am. Ceram. Soc.* 78 (1995) 3409–3411.
- [17] B.H. Sun, T.X. Fan, D. Zhang, T. Okabe, Microstructure analysis of morph-genetic SiC/C ceramics from wood, *J. Adv. Mater.* 37 (2005) 76–80.
- [18] A. Zampieri, H. Sieber, T. Selvam, G.T.P. Mabande, W. Schwieger, F. Scheffler, M. Scheffler, P. Greil, Biomorph cellular SiSiC/zeolite ceramic composites: from rattan palm to bioinspired structured monoliths for catalysis and sorption, *Adv. Mater.* 17 (2005) 344–349, <https://doi.org/10.1002/adma.200400672>.
- [19] D. Verboekend, J. Pérez-Ramírez, Desilication mechanism revisited: highly mesoporous all-silica zeolites enabled through pore-directing agents, *Chem. Eur. J.* 17 (2011) 1137–1147, <https://doi.org/10.1002/chem.201002589>.
- [20] J. He, T. Kunitake, Preparation and thermal stability of gold nanoparticles in silk-templated porous filaments of titania and zirconia, *Chem. Mater.* 16 (2004) 2656–2661, <https://doi.org/10.1021/cm049548l>.
- [21] J.T. Chao, M.J.P. Biggs, A.S. Pandit, Diatoms: a biotemplating approach to fabricating drug delivery reservoirs, *Expert Opin. Drug Deliv.* 11 (2014) 1687–1695, <https://doi.org/10.1517/17425247.2014.935336>.
- [22] S. Liu, J. He, Facile fabrication of porous titania microtube arrays by replication of human hair, *J. Am. Ceram. Soc.* 88 (2005) 3513–3514, <https://doi.org/10.1111/j.1551-2916.2005.00615.x>.
- [23] K. Keren, R.S. Berman, E. Braun, Patterned DNA metallization by sequence-specific localization of a reducing agent, *Nano Lett.* 4 (2004) 323–326, <https://doi.org/10.1021/nl035124z>.
- [24] E. Dujardin, C. Peet, G. Stubbs, J.N. Culver, S. Mann, Organization of metallic nanoparticles using tobacco mosaic virus templates, *Nano Lett.* 3 (2003) 413–417, <https://doi.org/10.1021/nl034004o>.
- [25] M.W. Anderson, S.M. Holmes, N. Hanif, C.S. Cundy, Hierarchical pore structures through diatom zeolitization, *Angew. Chem. Int. Ed.* 39 (2000) 2707–2710.
- [26] Y. Lei, Q. Wu, C.M. Clemons, F. Yao, Y. Xu, Influence of nanoclay on properties of HDPE/wood composites, *J. Appl. Polym. Sci.* 106 (2007) 3958–3966, <https://doi.org/10.1002/app.27048>.
- [27] T. Nypelö, H. Pynnönen, M. Österberg, J. Paltakari, J. Laine, Interactions between inorganic nanoparticles and cellulose nanofibrils, *Cellulose* 19 (2012) 779–792, <https://doi.org/10.1007/s10570-012-9656-x>.
- [28] T. Nypelö, O. Rojas, Functionalization of cellulose fibers by mineral and ceramic particle deposition, *Am. Ceram. Bull.* 91 (2012) 28–31.
- [29] J. Kostjukovs, A. Trubaca-Boginska, A. Actins, Method for Separation of Submicron Particles of Illite Mineral from Illite Clay, 2015. EP2840063.
- [30] G. Sedmale, M. Randers, M. Rundans, V. Seglins, Application of differently treated illite and illite clay samples for the development of ceramics, *Appl. Clay Sci.* 146 (2017), <https://doi.org/10.1016/j.clay.2017.06.016>.
- [31] C.A. Schneider, W.S. Rasband, K.W. Eliceiri, NIH Image to ImageJ: 25 years of image analysis, *Nat. Methods* 9 (2012) 671–675, <https://doi.org/10.1038/nmeth.2089>.
- [32] Iso 15705:2002, Water Quality — Determination of the Chemical Oxygen Demand Index (ST-COD) — Small-Scale Sealed-Tube Method, 2002.
- [33] S. Jemai, A. Ben Haj Amara, J. Ben Brahim, A. Plançon, Etude structurale par diffraction des RX et spectroscopie IR des hydrates 10 et 8.4 Å de kaolinite, *J. Appl. Crystallogr.* 32 (1999) 968–976, <https://doi.org/10.1107/S0021889899008602>.
- [34] H. Ming, Modification of kaolinite by controlled hydrothermal deuteration - a DRIFT spectroscopic study, *Clay Miner.* 39 (2004) 349–362, <https://doi.org/10.1180/0009855043930140>.
- [35] K.L. Konan, C. Peyratout, A. Smith, J.P. Bonnet, P. Magnoux, P. Ayrault, Surface modifications of illite in concentrated lime solutions investigated by pyridine adsorption, *J. Colloid Interface Sci.* 382 (2012) 17–21, <https://doi.org/10.1016/j.jcis.2012.05.039>.
- [36] M.H. Abd Aziz, M.H.D. Othman, N.A. Hashim, M.R. Adam, A. Mustafa, Fabrication and characterization of mullite ceramic hollow fiber membrane from natural occurring ball clay, *Appl. Clay Sci.* 177 (2019) 51–62, <https://doi.org/10.1016/j.clay.2019.05.003>.
- [37] S. Gunasekaran, G. Anbalagan, S. Pandi, Raman and infrared spectra of carbonates of calcite structure, *J. Raman Spectrosc.* 37 (2006) 892–899, <https://doi.org/10.1002/jrs.1518>.
- [38] J. Madejová, H. Pálková, P. Komadel, Behaviour of Li⁺ and Cu²⁺ in heated montmorillonite: evidence from far-, mid-, and near-IR regions, *Vib. Spectrosc.* 40 (2006) 80–88, <https://doi.org/10.1016/j.vibspec.2005.07.004>.
- [39] I. Plusnina, *Infrared-spectra for Silicates*, Moscow State University, Moscow, 1967.
- [40] L. Hou, L. Wang, S. Royer, H. Zhang, Ultrasound-assisted heterogeneous Fenton-like degradation of tetracycline over a magnetite catalyst, *J. Hazard Mater.* 302 (2016) 458–467, <https://doi.org/10.1016/j.jhazmat.2015.09.033>.